Astron. Astrophys. 348, 1012–1019 (1999)

ASTRONOMY AND ASTROPHYSICS

Mid-infrared spectral evolution of thermally annealed amorphous pyroxene

J.R. Brucato[1], **L. Colangeli**[1], **V. Mennella**[1], **P. Palumbo**[2], **and E. Bussoletti**[2]

[1] Osservatorio Astronomico di Capodimonte, via Moiariello 16, I-80131 Napoli, Italy
[2] Istituto Universitario Navale, via A. De Gasperi 5, I-80133 Napoli, Italy

Received 9 April 1999 / Accepted 7 June 1999

Abstract. Ground and space born spectroscopic observations have shown that crystalline Mg-rich silicates are among the main components of cometary grains. We have produced amorphous Mg-rich pyroxene particles by laser evaporation of natural mineral. Thermal annealing of the material has been performed at 800 and 1000 °C for different time lags. Composition and morphological properties of the samples have been characterized. Mid–infrared spectroscopy has been used to monitor the structural evolution with annealing from amorphous to crystalline phase. The activation temperature of the amorphous to crystalline transition derived from our measurements is about 47,500 K. This result suggests that crystalline silicates, observed in comets, may have been produced by long term exposure of the amorphous grains to temperature higher than 770 K during the pre–cometary phase.

Key words: comets: general – methods: laboratory – techniques: spectroscopic

1. Introduction

Silicates are among the main components of dust in different astronomical environments. Amorphous silicates have been invoked to explain typical infrared bands observed towards lines of sight that test the diffuse interstellar medium (e.g. Whittet et al. 1997) or young stellar objects (Jäger et al. 1994). Recently, ISO (Infrared Space Observatory) spectra of disks surrounding young stars (e.g. Malfait et al. 1998), of isolated Herbig Ae/Be stars (Waelkens et al. 1996), red supergiants, asymptotic giant branch, and post-AGB stars (Waters et al. 1996) and planetary nebulae with Wolf–Rayet central stars (Waters et al. 1998) have shown a variety of emission features that can be attributed to silicates in crystalline phase.

The presence in comets of a crystalline silicate component was already detected in the infrared spectrum of comet P/Halley 1986 III. A strong 11.3 μm peak was indeed attributed to crystalline olivine particles (Campins & Ryan 1989). The presence of the double peak at 9.8 and 11.3 μm indicates that amorphous and crystalline silicates coexist. Hanner et al. (1994a), by the infrared spectral analysis of several comets, revealed that a variety of emission features exists. Colangeli et al. (1996) fitted the cometary spectra revised by Hanner et al. (1994a, 1994b) by using laboratory spectra of different classes of crystalline silicates.

The recent passage of comet Hale-Bopp C/1995 O1 has provided the first opportunity to observe a new long period comet belonging to the Oort Cloud. Thanks to the use of ISO, it has been possible to measure the emission of the cometary coma grains in a wide infrared spectral range (6–45 μm) (Crovisier et al. 1997). A rich variety of strong emission features was measured and attributed mainly to the presence of crystalline Mg-rich olivine (forsterite) grains (Brucato et al. 1999). Ground–based observations, performed when comet Hale–Bopp was close to perihelion by Wooden et al. (1999), indicate that a further component of crystalline pyroxene grains is present. ISO observation programs have also considered several short period comets of the Jupiter family (e.g. Crovisier et al. 1999). The presence in the 5–17 μm spectrum of 103P/Hartley 2 of the 11.3 μm peak (Crovisier et al. 1999) indicates that crystalline silicates are present also in Kuiper belt comets.

Oort Cloud comets are believed to be icy planetesimals that formed in the outer solar nebula between Jupiter's and Neptune's orbits (5–30 AU) and were scattered by gravitational interactions with the planets to the very distant orbits of the Oort Cloud (Oort 1950, Kuiper 1951). Safronov (1969) proposed that Uranus and Neptune, instead of Jupiter and Saturn, could provide considerable dynamical scattering to form the Oort Cloud. This scenario was confirmed by Fernandez & Ip (1981, 1983) calculations. Since Jupiter tends to scatter planetesimals into gravitationally unbound orbits, most Oort Cloud comets probably originated well outside the Jupiter's orbit or formed at Oort Cloud distances (Hills 1982, Hills & Sandford 1983, Bailey 1987). The Kuiper belt comets presumably formed in place as icy planetesimals just beyond the Neptune's orbit and so they sample even more distant regions of the solar nebula, out to about 45 AU (Weissman 1995). In this scenario comets should reflect mostly unchanged the composition of the interstellar medium.

More recently the discovery of the 1996 PW object, apparently asteroidal but with orbital elements typical of long-period comets, implies that 1% of the Oort population should be as-

Send offprint requests to: J.R. Brucato
Correspondence to: brucato@na.astro.it

teroids (Weissman & Levison 1997). This suggests that Oort Cloud's objects could be formed by materials coming from as close as the asteroid belt in the primordial solar nebula. An interesting implication is that cometary materials suffered higher temperatures than previously supposed.

The presence of crystalline olivine and pyroxene as cometary grains is difficult to explain if comets were formed in the outer region of the solar nebula, where ISM amorphous silicates were presumably preserved unaltered. The cometary materials could have been processed thermally in the early phase of the presolar nebula, but it is not clear to what extent the interstellar dust has been thermally modified before comet formation. If the precometary dust suffered high enough thermal processing for sufficiently long times, structural changes of the silicate materials could have occurred. Structural trasformations imply variations of the optical properties.

A comprehensive analysis of the spectral features of crystalline silicates has recently been reported by Jäger et al. (1998), with reference to the presence of these materials in comets and other astrophysical environments. In the framework of the transformations mentioned above, it is necessary to investigate in laboratory the structural modifications induced on amorphous materials by thermal annealing. In particular, the infrared spectral evolution as a function of annealing temperature and of the processing time is of main interest. Laboratory annealing measurements have been performed by Day (1974), Day & Donn (1978), Nuth & Donn (1982), and Hallenbeck et al. (1998) on silicate smokes produced by vapor phase condensation and the amorphous to crystalline transition has been investigated by infrared spectroscopy.

In our work we have produced an amorphous silicate by using a different experimental method, the laser vaporization. With this technique it is possible to obtain a homogeneous amorphous material with nearly the same elemental composition of the starting minerals. In particular, we have used the crystalline Mg-rich member of the pyroxene class (enstatite) as parent material. The samples have been characterized in terms of chemical and morphological properties. The infrared spectra between 4 and 25 μm have been obtained at different times and temperatures of annealing.

In Sect. 2 we describe the experimental approach used for sample preparation and analysis. Sect. 3 is devoted to the presentation of results, which are discussed in Sect. 4. Finally, in Sect. 5 we draw same astrophysical considerations.

2. Experimental

In order to synthetize small amorphous grains from a natural crystalline enstatite bulk sample, we applied the laser evaporation technique, already used in previous cosmic dust analogue experiments (e.g. Stephens & Rusell 1979, Scott & Duley 1996).

In our experiments we used an infrared power solid–state laser Nd–YAG (Continuum Surelite II), whose main characteristics are summarised in Table 1. The power density emitted in one laser pulse (5–7 ns duration) in the Q-switch mode is $\sim 10^8$ W cm^{-2}. To prepare the targets for laser bombardment, fragments of the bulk pure silicate mineral were finely ground in an agata mortar. Pellets of 13 mm in diameter were obtained by pressing the dust at 15 tons between two stainless steel disks with optically worked surfaces. The pellets present a relatively flat and smooth surface. The target surface formed an angle of 45°with respect to the laser pulse direction, allowing the collection of the vapor condensate normally to the target. The experiments were carried out in O_2 atmosphere at a fixed pressure of 10 mbar. Crystalline grain samples were prepared by grinding the natural enstatite mineral in the agata mill. Both laser produced and ground crystalline sample (hereafter labelled as ENSA and ENSC, respectively) were sedimentated in ethanol, to select the smallest grains.

Table 1. Characteristics of the Nd-YAG (Continuum Surelite II) laser used in our experiments.

Frequency	10 Hz
Wavelength	1064 nm
Energy	650 mJ
Q-switch delay	185μs
pulsewidth	5–7 ns
rod diameter	7 mm

The annealing experiments were performed in a ceramic oven in vacuum (P$\leq 10^{-6}$ mbar) at temperatures of 800 °C and 1000 °C. The heating rate and the stability in temperature was controlled by an electronic device connected to a termocouple located on the sample holder. An heating rate up to $\sim$23 °C min^{-1} was used. About 18 (30) min of stabilisation were needed before the final value of 800 (1000) °C were reached. On the rising temperature ramp the maximum reached value was 819 (1017) °C. After stabilisation, different heating times were maintained; for each experiment a fresh amorphous sample was used. Unfortunately, the amount of material obtained after annealing was not enough to apply the sedimentation process and select the smallest grains only. Then, the samples used for spectral analyses after thermal processing contain a (minor) fraction of large grains.

The morphological characterization of the samples was performed by means of a Field Emission Scanning Electron Microscope (FESEM – mod. Stereoscan FE360), with a spatial resolution of 2 nm. To prepare samples for FESEM analysis a solution of crystalline grains and ethanol was deposited on a silicon wafer chip fixed on an aluminium stub. Laser produced grains were collected on a similar substrate exposed to the dust flux during bombardment. The samples were coated with a Cr film, in order to avoid their charging and to obtain the best resolution. The morphology was observed and the size distribution and average dimension were determined. Ten images at different magnifications (M=1,000–50,000) were acquired, for each sample and on different areas of the sample. The size distribution was obtained by counting the grains in the class of size d detectable with each magnification and by assuming a uniform space distribution. In order to avoid frequency underestimation of the smallest grains, we started with the magnification which allowed to resolve the smallest particles. Then, the magnifica-

tion was progressively reduced by keeping constant the product $M \cdot d$, i.e. the spatial resolution. Since the crystalline grain shape is very irregular, we considered the maximum elongation as the measure of the typical size of the particles. The vaporised grains appear rather spherical. Since they are often organized in chain–like structures it was necessary to use an image analysis software (Global Lab Image) in order to measure their diameter.

The chemical composition of the samples was studied by means of an Energy Dispersive X-ray (EDX) detection system, linked to the FESEM. For this kind of analysis grains were uniformly deposited on a carbon stub. The EDX spectra were acquired on 10 different areas of each dust sample and the average elemental content was measured. An appropriate software was used to evaluate the mass concentration of the elements by comparing the collected X-ray spectra with those of standard samples. To analyse the EDX data we adopted the criteria suggested by Papike (1987). For pyroxene samples: 1) the oxide sum should be approximately 100%; 2) the Si ion number should be ≤ 2; 3) Ca + Na ion number must be ≤ 1; 4) the analysis is based on a six-oxygens normalization; 5) the total number of cations must be ≤ 4.

In order to study the optical properties of the materials between 2.5 and 25 μm, trasmission spectra of the dust samples were collected at the spectral resolution of 2 cm^{-1} by means of a FT–IR interferometer (mod. Bruker Equinox 55). Spectra of dust samples embedded in KBr pellets were acquired. By using blank KBr pellets as reference the mass extinction coefficient, $K(\lambda)$, was derived. The final spectra are the average of many measurements.

3. Results

The results of our elemental analysis are reported in Table 2. The automatic minimization process used by the EDX analysis software produces concentration fluctuations due to the variability of the EDX system. In our analysis the total percentage concentration is in the range 93–101%. It should be noted that all samples show the presence of Cr, mainly due to the coating film, even if some fraction of Cr could be a natural component of the materials.

Minerals of the pyroxene group (XYZ_2O_6 where X = Ca, Mn^{2+}, Fe^{2+}, Mg, Na, Li; Y = Mn^{2+}, Fe^{2+}, Mg, Fe^{3+}, Al, Cr, Ti; and Z = Si, Al) crystallize in a variety of space groups, which differ in the links among octahedral and tetrahedral layers. Between the various pyroxene end-members, enstatite $Mg_2Si_2O_6$ (En), ferrosilite $Fe_2Si_2O_6$ (Fs) and, wollastonite $Ca_2Si_2O_6$ (Wo), our ENSC sample is En87Fs8Wo5. The Ca content is just at the border of orthopyroxene and clinopyroxene pigeonite and ENSC has quite a bit of Al. We notice that the ratios of the main elements, before and after the laser vaporisation, are preserved, within some percent; e.g. the (Fe + Mg)/Si ratio varies of 5% at most. After vaporization the chemical composition is that of En84Fs12Wo4, with an higher content of Fs with respect to the crystalline sample. After thermal annealing at 800 and 1000°C the composition returns to about the initial value En87Fs9Wo4. Thus, our analysis demonstrates that the laser evaporation does not affect significantly the relative elemental composition.

Table 2. Oxide concentrations (%) and ion numbers of natural crystalline (ENSC), laser vaporised (ENSA) and thermally annealed (ENST, at 800 °C for 311^h) samples.

	ENSC	ENSA	ENST
Major Oxides			
FeO	5.35	6.81	5.90
Cr_2O_3	3.68	4.56	1.73
CaO	2.64	1.76	2.19
SiO_2	52.39	46.36	49.63
MgO	33.02	26.57	31.51
Al_2O_3	4.04	6.94	3.17
Total	101.12	93.00	94.19
Number of ions			
Fe	0.157	0.217	0.184
Cr	0.100	0.136	0.051
Ca	0.099	0.074	0.087
Si	1.820	1.766	1.858
Mg	1.709	1.504	1.746
Al	0.163	0.313	0.134
O	6.000	6.000	6.000

As the spectral behaviour of samples depends significantly on the grain morphology (e.g. Bohren & Huffman 1983), their study is important to correctly interpret results about optical properties. In particular, the Rayleigh limit ($2\pi a/\lambda \ll 1$, with a grain radius) must be satisfied in the spectral range of interest in order to consider the scattering negligible and the observed features due to pure absorption.

The sample obtained after sedimentation of laser produced grains is a collection of both isolated spheres and agglomerates. The FESEM analysis has shown the maximum grain diameter after sedimentation to be 1.2 μm. However, most of the grains fall in the range up to 75 nm (Fig. 1). The size distribution was fitted (correlation index, r = 0.97) by a log–normal (LN) function:

$$f_{LN}(d) = \frac{A}{ln\sigma} exp\left(-\frac{(lnd - ln\bar{d})^2}{2(ln\sigma)^2}\right) \quad (1)$$

where A is a normalization coefficient, d the particle diameter and σ the standard deviation (see Fig. 1). The best fit to the size distribution by f_{LN} is obtained for $\sigma = 1.32$ nm and $\bar{d}$=23.5 nm. The size distribution of ground crystalline grains (Fig. 2) follows a power–law (PL):

$$f_{PL}(d) = Ad^{-p} \quad (2)$$

where A is a normalization coefficient, d is the grain diameter and p is the power index. The best fit to the size distribution by f_{PL} is obtained for $p = 2.8$ with a correlation index $r = -0.96$ and the average grain diameter is $\bar{d}$=0.2 μm. The overall size range is wider than that of the amorphous sample (maximum diameter=1.7 μm).

Fig. 3 shows the comparison of the infrared spectra of laser produced (ENSA) and crystalline (ENSC) samples. The rel-

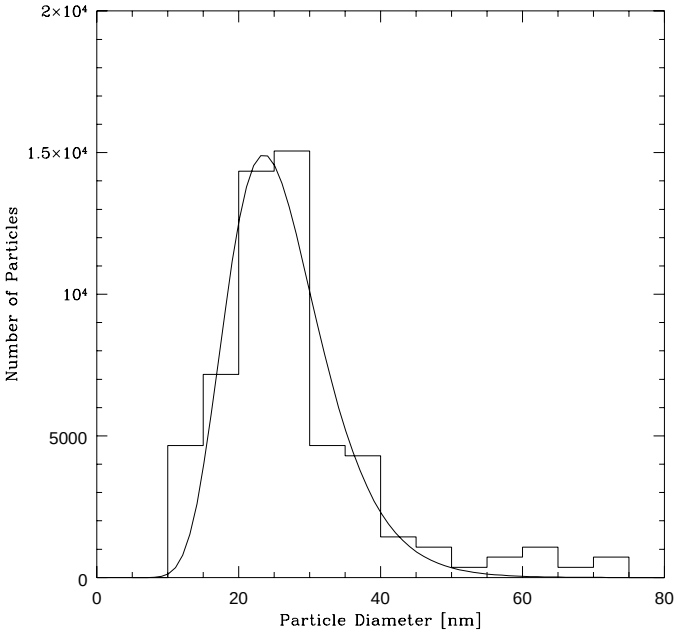

Fig. 1. Size distribution of amorphous grains, ENSA, sedimentated in ethanol ($\bar{d}$=23.5 nm). Grains with diameters above 75 nm are only a few percent of the total number and have been omitted from the figure for clarity. The continuous line is the best fit log-normal function ($\sigma = 1.32$ nm).

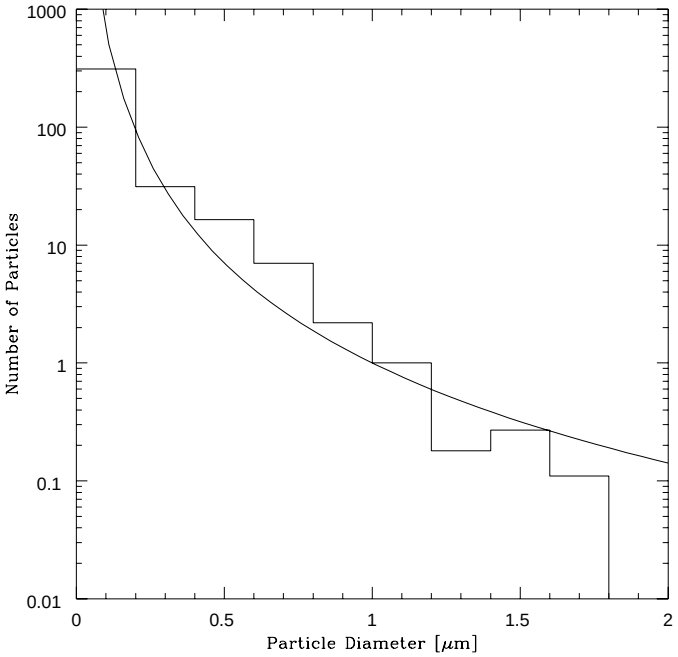

Fig. 2. Size distribution of crystalline enstatite grains, ENSC, sedimentated in ethanol. The continuous line is the best fit power law function (power index p=2.8; $\bar{d}$=0.2 μm).

ative error on $K(\lambda)$ is of the order of 3%. The spectrum of ENSC presents bands with a fine structure, absent in the ENSA spectrum, which shows two broad bands peaked at 9.89 and 19.21 μm, typical of amorphous silicates.

Table 3. Peak positions of amorphous enstatite after thermal annealing. The peaks of crystalline (ENSC) and amorphous (ENSA) enstatite are reported for comparison.

		800 °C				1000 °C	
ENSA	19^h	24^h	48^h	144^h	311^h	7^m	ENSC
–	–	9.43	9.38	9.34	9.34	9.37	9.33
9.89	9.91	9.91	9.91	9.91	9.93	9.91	9.83
–	–	10.49	10.53	10.56	10.53	10.56	10.57
–	–	–	11.07	11.14	11.13	11.21	11.13
–	–	–	–	–	–	–	11.56
–	13.81	13.75	13.77	13.68	13.75	13.81	13.79
–	14.46	14.59	14.48	14.53	14.53	14.55	14.48
–	–	15.46	15.46	15.53	15.55	15.53	15.46
–	–	–	16.44	–	16.36	–	–
–	18.55	18.52	18.72	18.29	18.42	18.39	18.52
19.21	19.46	19.57	19.57	19.68	19.53	19.79	19.91
–	–	–	20.70	20.70	20.87	20.87	21.52
–	–	–	23.10	23.52	23.15	23.73	24.58

The peak positions measured for ENSC (see last column of Table 3) differ at most of 1% with respect to those reported by Jäger et al. (1998), who have studied in the laboratory similar materials. The small differences may be attributable to slightly different chemical composition of the analysed silicates. Peaks at 4.25, 6.26 and 6.94 μm, observed in our spectra, are due to atmospheric contaminants (e.g. water vapour) both in gaseous form and adsorbed onto the samples. These features result not fully compensated in the ratio between the spectrum of the sample in KBr and that of blank KBr.

The spectroscopic investigation allowed us to evidence structural modifications induced by thermal annealing. The results are shown in Figs. 4 and 5 and the peaks evolution is summarized in Table 3. Actually, the $K(\lambda)$ profile shows significant variations with annealing time and temperature, which can be related to an evolution towards a more ordered lattice configuration. After 19^h of annealing at 800 °C, the maximum at 9.89 μm evolves and two side shoulders appear, even if the overall FWHM of the band does not vary significantly. After 24^h, three separate peaks are observed at 9.43, 9.91 and 10.49 μm, with similar intensities. As the annealing time is increased up to 48^h, 144^h and 311^h, the position of the peaks remains rather stable (see Table 3), but their intensity and sharpness evolves: the peaks at 9.4 and 10.5 μm overcome in intensity the 9.89 μm band. Moreover, a well defined peak at 11.1 μm appears. The band at 19.21 μm follows a similar evolution. After 19^h, a new peak appears at 18.55 μm and after 24^h the peak at 19.57 μm overwhelms in intensity the 18.52 μm feature. As long as the annealing time increases, the peak positions slightly change (see Table 3) and the bands sharpen. Other features, between the two main 10 and 20 μm bands, do appear (at 13.8, 14.5, 15.5 and 16.4 μm) and become more and more intense with annealing time. At 1000 °C, the evolution of the IR spectrum is much faster. After 7^m the spectrum shows a shape similar to that obtained after 311^h at 800 °C (Fig. 5). The peaks fall nearly at the same positions as for the crystalline sample.

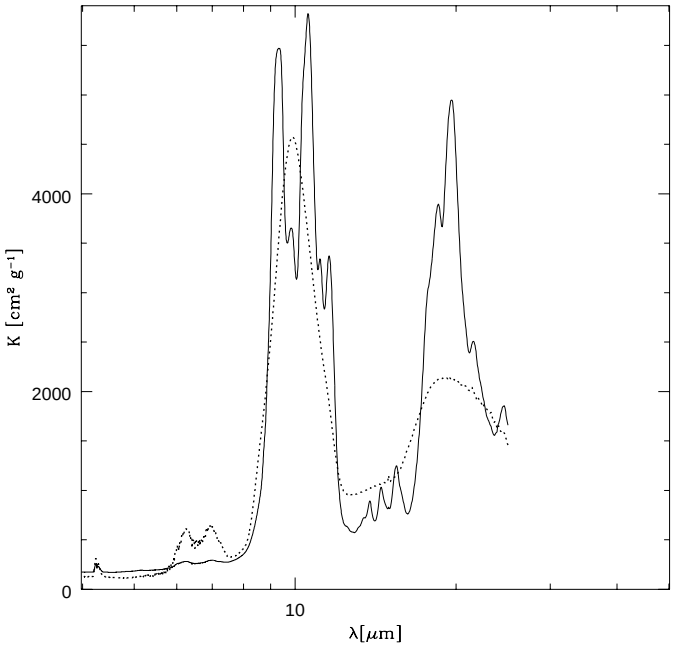

Fig. 3. Mass absorption coefficient of crystalline (ENSC, continuous line) and amorphous (ENSA, dashed line) enstatite.

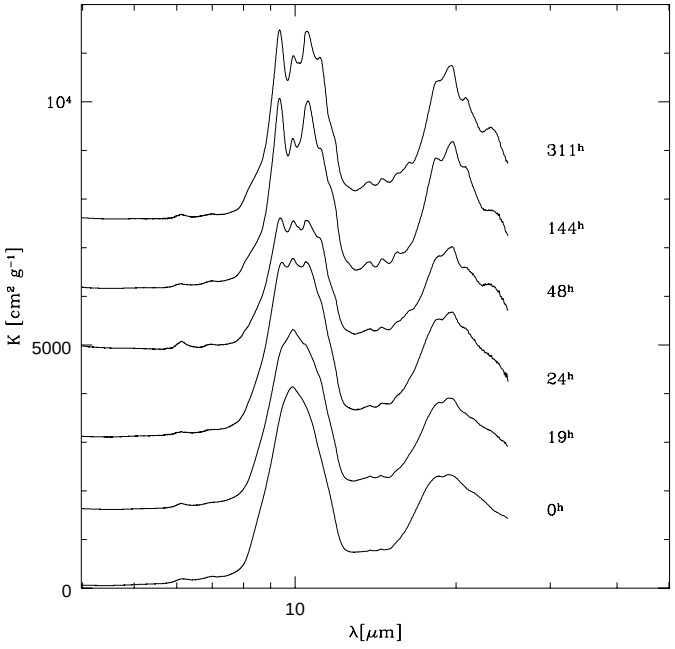

Fig. 4. Mass absorption coefficient of amorphous not sedimented enstatite grains annealed at 800°C as a function of time. The spectra annealed are upper shifted each other with respect to the ordinate scale by 1500 $cm^2\ g^{-1}$ for sake of clarity.

FESEM analysis before and after thermal annealing shows some trasformation in the morphology of the grains (Fig. 6). ENSA grains have a nearly spherical shape, as typical of the vapour condensed amorphous grains (see following section). After thermal processing the structure changes in a more ordered arrangement and spherical grains evolve towards a more irregular shape.

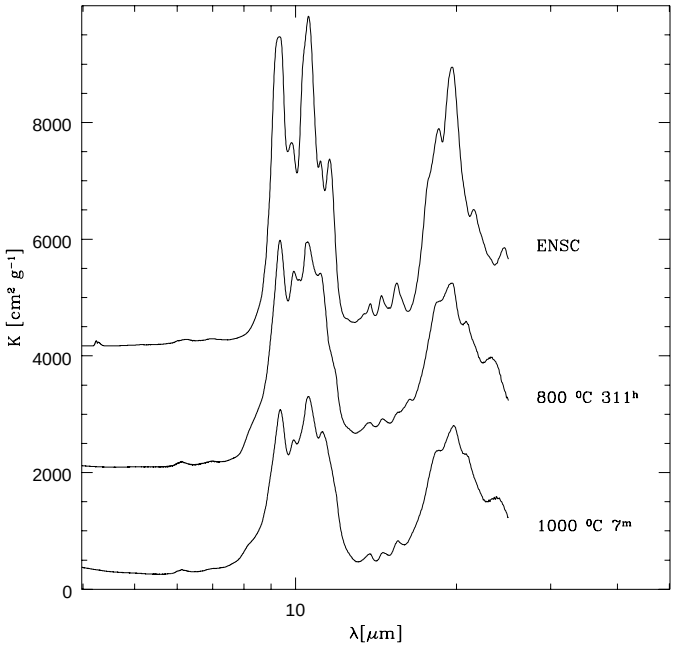

Fig. 5. Mass absorption coefficient of amorphous not sedimented enstatite grains annealed at 1000 °C for 7^m. The spectrum obtained for an annealing time of 311^h at 800 °C and that of crystalline enstatite (ENSC) are reported for comparison. The ENSC and 800 °C spectra are upper shifted each other with respect to the ordinate scale by 2000 $cm^2\ g^{-1}$ for sake of clarity.

4. Discussion

The laser vaporization is a useful technique to produce amorphous grains. The interaction process between laser radiation and target material depends on the laser power, the material absorbitivity at the wavelength of the laser emission and the thermal properties of the target. Species with low thermal diffusivity and high absorbitivity reach a concentration of thermal energy at the target surface and, thus, high peak temperatures. High power density lasers, as that we have used, produce a plasma leading to beam energy absorption by inverse Bremsstrahlung above the material surface. If the material temperature rises sufficiently above the boiling point, evaporation occurs and material is removed as vapour and ejecta. The temperature conditions to allow evaporation are usually reached in a short time, which depends on the laser power density, thermal diffusivity and sublimation heat of the material. Generally, these quantities vary with the temperature. The laser beam – material interaction causes a heat distribution in the target and the generation of energetic species owing to the formation of the plasma and its subsequent expansion.

In the presence of an atmosphere the evaporation process causes hot atoms to lose their energy by collisions with the cold gas atoms. The collision mean free path for an O_2 atmosphere at 10 mbar (conditions used in our experiment) is approximately

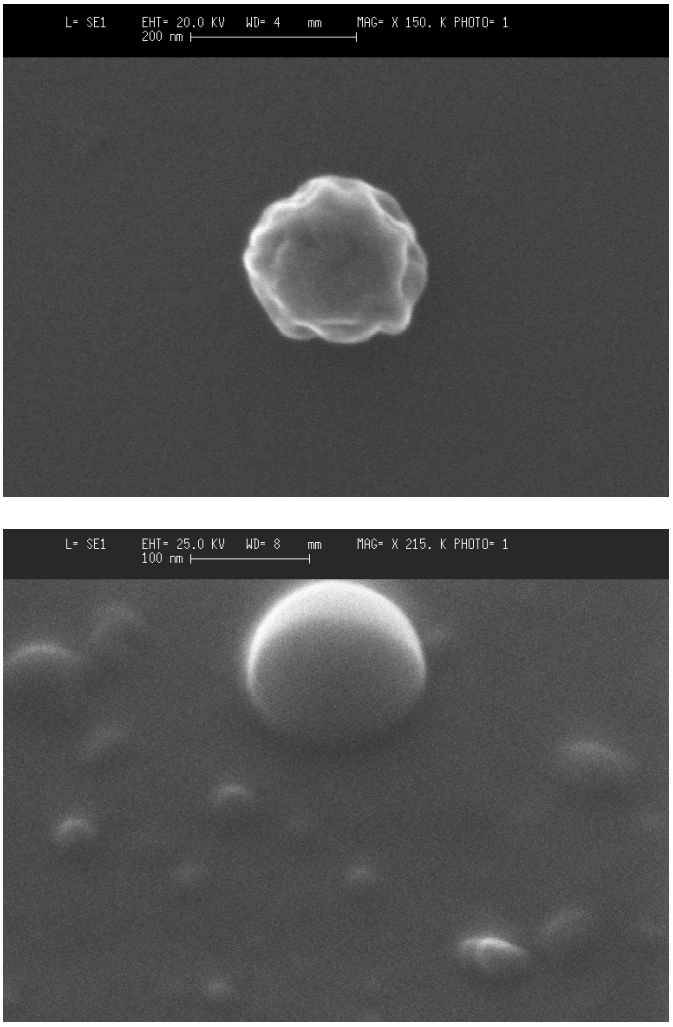

Fig. 6. FESEM images of amorphous enstatite produced by laser evaporation (*bottom figure*) and after annealing at 1000 °C for 7^m (*top figure*).

10^{-4} cm. The high expansion velocity (10^4–10^5 cm s^{-1}) of the hot gas and the collision cooling mechanism favour the supersaturation of the vapour. These conditions are appropriate to produce condensation. The produced particles have a size distribution and an average size that depend on the pressure and the molecular weight of the cooling gas and on the laser power density (Stephens 1980). The particle sizes decrease as the gas pressure inside the evaporation chamber is reduced, due to the faster expansion of the laser–produced vapor plume in a lower pressure atmosphere.

The structure, shape and size distribution of the condensed materials depend on the velocity of the quenching of the hot atoms after evaporation. At 10 mbar of pressure, the cooling collisions of the hot atoms are fast. Under these conditions, thermodynamics predicts (Abraham 1974) that the critical diameter of the nucleating particles is very small (≤ 1 nm). Once the nucleation has taken place, the particles can grow by absorption of atomic vapour or by coalescence, if the particles behave as a liquid (Granqvist & Buhrman 1976). The grain shape depends on the surface tension of the liquid particles, from which the grains are formed, times the surface area. The final shape is reached when this quantity has a minimum (Gibbs–Wulff criterion). If the surface migration time, t_s, of the impinged atoms is greater than the time interval, t_i, between two consecutive arrivals of atoms from the vapour phase onto the grain surface, the atoms have no time to reach an ordered structure and an amorphous grain is formed. The possibility to obtain a crystalline grain depends on the temperature and on the activation energy of the material. In the absence of a crystalline structure the Gibbs–Wulff criterion predicts a spherical shape, as it is observed for our laser vaporised samples. After formation, the coagulation process produces chain like aggregates.

The atoms of the amorphous material subject to thermal annealing may occupy various stable configurations, more or less ordered at long and short ranges. When the mean energy of the atoms is sufficiently high to overcome the energy barriers, they can move towards a more energetically stable configuration within the lattice, characterized by a local energy minimum. By this process the material gradually moves from an amorphous to a crystalline structure. The structural changes depend on the chemical composition of the amorphous material. The time, t_{hop}, which the atoms spend to reach a more favorable long–range order inside the lattice is defined as (Lenzuni et al. 1995):

$$t_{hop} = \nu^{-1} exp\left(\frac{E_a}{KT}\right) \quad (3)$$

where ν is a characteristic vibrational frequency, and E_a is the activation energy of the amorphous–crystalline transition. In our annealing experiments t_{hop} is 311^h and 7^m at 800 and 1000 °C, respectively. In fact, for longer times no significant spectral variation is observed. Taking for ν the average value $2.5 \cdot 10^{13}$ s^{-1}, intermediate between those associated with the stretching and bending modes of the SiO_4 tetrahedron, the average value for the activation temperature obtained from our experiments is $E_a/K = 47,500$ K within a percent error of 2%.

The absence of new bands in the thermally processed samples, with respect to those present in the ENSC spectra, indicates that chemical fractionation has not occurred. Then, the obtained activation temperature is that of a pirossenic silicate chemically homogeneous with the composition shown in Table 2. The value of the activation temperature obtained in this work is 14% higher than that (41,000 K) estimated by Lenzuni et al. (1995) starting from the data obtained by Nuth & Donn (1982) for the annealing of magnesium-silicate smokes. This difference can be probably due to compositional and structural differences between the samples.

The differences in the peak ratios between annealed samples and ENSC are probably due to size effects. The spectral contrast of a band is reduced as the size of the grains increases and the Rayleigh limit is overcome. In fact, the larger grains provide a minor contribution to the band intensity and the mass absorption coefficient results less intense.

We recall that our spectra are obtained for samples embedded in KBr and are not corrected for matrix effects. These may affect peak positions, band widths and intensities to some extent (Dorschner et al. 1978). However, Colangeli et al. (1995) showed that the peak shift is limited to about 1%.

5. Astrophysical application

The results obtained in this work confirm that amorphous pyroxene with Mg–rich composition presents high activation temperature. This prevents possible crystallization either in the outer region of the Solar nebula and during the passage at perihelion of comets. Structural changes occur for time scales $\leq 10^6$ yr, if temperatures are ≥ 770 K. This is in agreement with various experimental results concerning thermal annealing of amorphous grains produced by vapour condensation with different chemical composition. Hallenbeck et al. (1998) have shown that, once annealed, the magnesium silicate smokes cross a stall phase identified by the time interval in which the infrared spectra do not change, while the atoms reach a more ordered configuration. The spectrum obtained by these authors at 1027 K after 192^h of annealing corresponds to an activation temperature of 45,500 K, 4% lower than that obtained in our experiment. This is probably due to compositional differences. In fact, the spectrum obtained after annealing by Hallenbeck et al. resembles a mixture of silica and crystalline olivine.

The results obtained for the activation temperature have an impact on the modelling of the possible evolution of materials in the proto–solar system. Up to now it is not clear to what extend the proto–solar accretion disk suffered mixing between the warmer inner and the cooler outer regions. According to the modelling by Stevenson (1990), in the steady state accretion disks of the solar nebula the fraction of material that suffered thermochemical processing at small radii depends only on one parameter: the ratio, *k*, between the eddy diffusivity and the eddy viscosity. If *k* was ≤ 1, most of the presolar nebula material survived unchanged. On the contrary, for $k > 1$ an appreciable fraction of material was processed. Prinn (1990) demonstrated that the contribution of non linear processes may further increase the mixing ratio of species in the solar nebula. Taking into account the high activation temperature, the latter scenario seems compatible with the detection of IR emission features due to crystalline silicate in cometary spectra (e.g. Campins & Ryan 1989, Hanner et al. 1994a, 1994b, Crovisier et al. 1997, 1999).

On the other hand, the shocks produced by proto–planet accretion can locally rise enough the temperature to vaporize or crystallize the silicates even at high heliocentric distances. These materials can be incorporated in comets without visiting the inner nebula (Prinn & Fegley 1988, Yung et al. 1988). However, up to now the efficiency of this process is still not clear.

Finally, pre–cometary grains suffered ion bombardment and UV irradiation in the interstellar medium at rates sufficient to alter the chemical and structural composition (e.g. Hagen et al. 1979, Kratschmer & Huffman 1979, Strazzulla & Johnson 1991). The amorphous silicates, processed in this way, could need activation energies lower than that measured in the laboratory. Then, the temperatures reached (some hundred degrees) during passage of comets at perihelion could become sufficient to produce the amorphous–crystalline transition.

The previous considerations clearly indicate that we are still far from a reasonable understanding of the material evolution in the proto–solar nebula and of the actual role played by driving processes. Further experiments are needed to simulate in detail the expected processes and to gain more confidence in the modelling of the Solar System early evolution.

Acknowledgements. This work has been supported under ASI, CNR and MURST contracts.

References

Abraham F.F., 1974, In: Homogeneous Nucleation Theory. Academic, New York
Bailey M.E., 1987, QJRAS 28, 242
Bohren C.F., Huffman D.R., 1983, In: Absorption and Scattering of Light by Small Particles. John Wiley and Sons Inc., New York
Brucato J.R., Colangeli L., Mennella V., Palumbo P., Bussoletti E., 1999, PSS 47, 773
Campins H., Ryan E.V., 1989, ApJ 341, 1059
Colangeli L., Mennella V., di Marino C., Rotundi A., Bussoletti E., 1995, A&A 293, 927
Colangeli L., Mennella V., Rotundi A., Palumbo P., Bussoletti E., 1996, A&A 312, 643
Crovisier J., Leech K., Bockelée-Morvan D., et al., 1997, Sci 275, 1904
Crovisier J., Encrenaz T., Lellouch E., et al., 1999, ESA SP-427, in press
Day K.L., 1974, ApJ 192, L15
Day K.L., Donn B., 1978, ApJ 222, L45
Dorschner J., Friedemann C., Gürtler J., 1978, Astron. Nachr. 299, 269
Fernandez J.A., Ip W.H., 1981, Icarus 47, 470
Fernandez J.A., Ip W.H., 1983, Icarus 54, 377
Granqvist C.G., Buhrman R.A., 1976, JAP 47, 2200
Hagen W., Allamandola L.J., Greenberg J.M., 1979, Ap&SS 65, 215
Hallenbeck S.L., Nuth III J.A., Daukantas P.L., 1998, Icarus 131, 198
Hanner M.S., Lynch D.K., Russell R.W., 1994a, ApJ 425, 274
Hanner M.S., Hackwell J.A., Russell R.W., Lynch D.K., 1994b, Icarus 112, 490
Hills J.G., 1982, AJ 87, 906
Hills J.G., Sandford M.T. II, 1983, AJ 88, 1519
Jäger C., Mutschke H., Bergemann B., Dorschner J., Henning Th., 1994, A&A 292, 641
Jäger C., Molster F.J., Dorschner J., et al., 1998, A&A 339, 904
Kratschmer W., Huffman D.R., 1979, Ap&SS 61, 195
Kuiper G.P., 1951, In: Hynck J.A. (ed.) Astorphysics. 357
Lenzuni P., Gail H.P., Henning Th., 1995, ApJ 447, 848
Malfait K., Waelkens C., Waters L.B.F.M., et al., 1998, A&A 332, L25
Nuth J.A., Donn B., 1982, ApJ 257, L103
Oort J.H., 1950, Bull. Astron. Inst. Neth. Vol. 11, 91
Papike J.J., 1987, RvGeo 25, 1483
Prinn R.G., Fegley B., 1989, In: Pollack J., Mattheews M. (eds.) Origin and evolution of planetary and satellite atmospheres. 78
Prinn R.G., 1990, A&A 348, 725
Safronov V.S., 1969, NASA TT–F–677, 206
Scott A., Duley W.W., 1996, ApJS 105, 401
Stephens J.R., Rusell R.W., 1979, ApJ 228, 780

Stephens J.R., 1980, ApJ 237, 450
Stevenson D.J., 1990, ApJ 348, 730
Strazzulla G., Johnson R.E., 1991, In: Comets in the post–Halley era. Vol. 1, 243
Waelkens C., Waters L.B.F.M., de Graauw M.S., et al., 1996, A&A 315, L245
Waters L.B.F.M., Molster F.J., de Jong T., et al., 1996, A&A 315, L361
Waters L.B.F.M., Beintema D.A., Zijlstra A.A., et al., 1998, A&A 331, L61
Weissman P.R., 1995, A&AR 33, 327
Weissman P.R., Levison H.F., 1997, ApJ 488, L133
Whittet D.C.B., Boogert A.C.A., Gerakines P.A., et al., 1997, ApJ 490, 729
Wooden D.H., Harker D.E., Woodward C.E., et al., 1999, ApJ 517, 1034
Yung Y.L., Friedl R.R., Pinto J.P., Bayes K.D., Wen J-S., 1988, Icarus 74, 121